Extracellular Vesicles in Human Skin: Cross-Talk from Senescent Fibroblasts to Keratinocytes by miRNAs

Lucia Terlecki-Zaniewicz[1,2], Vera Pils[1,2], Madhusudhan Reddy Bobbili[2], Ingo Lämmermann[1,2], Ida Perrotta[3], Tonja Grillenberger[1,2], Jennifer Schwestka[1,2], Katrin Weiß[1,2], Dietmar Pum[4], Elsa Arcalis[5], Simon Schwingenschuh[6], Thomas Birngruber[6], Marlene Brandstetter[7], Thomas Heuser[7,8], Markus Schosserer[2], Frederique Morizot[9], Michael Mildner[10], Eva Stöger[5], Erwin Tschachler[10], Regina Weinmüllner[1,2], Florian Gruber[1,10] and Johannes Grillari[1,2,8,11]

Extracellular vesicles (EVs) and their miRNA cargo are intercellular communicators transmitting their pleiotropic messages between different cell types, tissues, and body fluids. Recently, they have been reported to contribute to skin homeostasis and were identified as members of the senescence-associated secretory phenotype of human dermal fibroblasts. However, the role of EV-miRNAs in paracrine signaling during skin aging is yet unclear. Here we provide evidence for the existence of small EVs in the human skin and dermal interstitial fluid using dermal open flow microperfusion and show that EVs and miRNAs are transferred from dermal fibroblasts to epidermal keratinocytes in 2D cell culture and in human skin equivalents. We further show that the transient presence of senescent fibroblast derived small EVs accelerates scratch closure of epidermal keratinocytes, whereas long-term incubation impairs keratinocyte differentiation in vitro. Finally, we identify vesicular miR-23a-3p, highly secreted by senescent fibroblasts, as one contributor of the EV-mediated effect on keratinocytes in in vitro wound healing assays. To summarize, our findings support the current view that EVs and their miRNA cargo are members of the senescence-associated secretory phenotype and, thus, regulators of human skin homeostasis during aging.

INTRODUCTION

Extracellular vesicles (EVs) are versatile and ubiquitously present membranous particles that participate in intercellular communication by shuttling their functional cargo, such as proteins, RNA, or DNA, to recipient cells (Iraci et al., 2016). In the context of the skin, they have been found in ex vivo sections of the human papillary dermis (Cretoiu et al., 2015), at sites of age-related cutaneous disorders (Nakamura et al., 2016), at wounds (Huang et al., 2015), and in the stroma of human skin tumors (Jang et al., 2017). In addition, in vitro vesicular cross-talk has been observed between several types of skin cells, including keratinocytes, melanocytes, human dermal fibroblasts (HDF), dermal papilla cells, outer root sheath cells of the hair follicle, and microvascular endothelial cells (Lo Cicero et al., 2015; Huang et al., 2015; Merjaneh et al., 2017; Wäster et al., 2016; Zhou et al., 2018). However, nothing is known about EV-mediated cross-talk between skin fibroblasts and keratinocytes during cellular aging.

In the elderly, senescent cells have been observed in the dermis and in the epidermis (Ressler et al., 2006). Their accumulation with age and at sites of age-associated diseases contributes to cellular, molecular, and structural changes of the dermal and epidermal compartments, where they impair skin homeostasis, causing increased susceptibility for dermatological disorders (Velarde and Demaria, 2016; Waaijer et al., 2016).

Senescent cells are irreversibly growth arrested, partially de- or trans-differentiated, and the acquisition of the senescence-associated secretory phenotype (SASP) is discussed as the most potent contributor of senescent cells to organismal aging. The SASP consists of growth factors, cytokines, chemokines, matrix remodeling enzymes (Coppé et al., 2010), as well as lipids (Ni et al., 2016), and thereby creates a chronically inflamed and pro-tumorigenic

[1]Christian Doppler Laboratory for Biotechnology of Skin Aging, Vienna, Austria; [2]Department of Biotechnology, University of Natural Resources and Life Sciences, Vienna, Austria; [3]Department of Biology, Ecology and Earth Sciences, University of Calabria, Cosenza, Italy; [4]Department of Nanobiotechnology, University of Natural Resources and Life Sciences, Vienna, Austria; [5]Department of Applied Genetics and Cell Biology, University of Natural Resources and Life Sciences, Vienna, Austria; [6]HEALTH − Institut für Biomedizin und Gesundheitswissenschaften, Joanneum Research, Graz, Austria; [7]Vienna BioCenter Core Facilities GmbH, Vienna, Austria; [8]Austrian Cluster for Tissue Regeneration, Vienna, Austria; [9]Department of Biology & Women's Beauty, Chanel, Pantin, France; [10]Department of Dermatology, Medical University of Vienna, Vienna, Austria; and [11]Ludwig Boltzmann Institute for Experimental and Clinical Traumatology, Vienna, Austria

Correspondence: Johannes Grillari, Department of Biotechnology, BOKU - University of Natural Resources and Life Sciences, Muthgasse 18, A-1190 Vienna, Austria. E-mail: johannes.grillari@boku.ac.at

microenvironment (Schosserer et al., 2017). The selective removal of senescent cells improves tissue homeostasis and repopulation of the hair bulge niche (Yosef et al., 2016), postpones the onset and severity of age-associated diseases, and thereby extends life- and health span of mice (Baker et al., 2016). However, their elimination in acute wounds delays the healing process, leading to fibrosis and impaired granulation tissue formation (Demaria et al., 2014; Jun and Lau, 2010).

Recently, EVs and their miRNA cargo emerged as communicators of the SASP of human dermal fibroblasts (EV-SASP; Terlecki-Zaniewicz et al., 2018; Urbanelli et al., 2016). In the skin, the presence of specific miRNAs within different layers and cell types regulates the balanced mRNA to miRNA ratio to maintain functional homeostasis (Botchkareva, 2012). Therefore, it is not surprising that the fine tuning of overlapping wound healing phases and skin aging-associated changes are regulated by the transient or constitutive presence of specific miRNAs (Sonkoly et al., 2010).

Here we shed light on the existence of EVs in human skin ex vivo and investigate an EV-miRNA cross-talk from fibroblasts to keratinocytes in monolayers and in 3D skin models. Finally, we evaluate how small EVs (sEVs) derived from senescent fibroblasts influence keratinocyte differentiation and their scratch closure capacity in vitro.

RESULTS

Extracellular vesicles are present in the human skin

To address if EVs are present in human skin in vivo, skin sections were studied by transmission electron microscopy (TEM) and images confirmed the presence of EV-like structures within dermal cells, adjacent to dermal cells in extracellular collagen structures (Figure 1a and b), and within intracellular multivesicular bodies (Figure 1c). These structures also stained positive for the EV marker CD63 by immunogold labeling of resin-free ultrathin cryo-cut skin sections (Figure 1d).

In order to isolate sEVs from human skin, tissue biopsies from two independent donors were disintegrated using dispase, and sEVs contained in accessible material were purified (see scheme in Supplementary Figure S1a). Particles from this crude extract were enriched by using tangential flow filtration with a cut-off of 300 kDa (Supplementary Figure S1b). Median size was approximately 110 nm as determined by nanoparticle tracking analysis (Figure 1e). These particles were positive for EV-markers TSG101 and syntenin, as shown by western blot analysis. However, calnexin, which is expected to be absent in sEVs, was also detectable (Figure 1f and Supplementary Figure S1c and d). Therefore, we further purified the EV enriched, skin derived preparations using size exclusion chromatography (SEC). Thereby, the majority of particles was eluted in the first six fractions and pools of fractions 1 to 3 and 4 to 6 (SEC 1−3, SEC 4−6) were prepared, and particle number was analyzed by nanoparticle tracking analysis, showing enrichment of particles in SEC 1−3, whereas lower numbers were recovered in fractions SEC 4−6 (Figure 1g); however, particle size of the fractions did not differ significantly (Figure 1h). These were then analyzed by western blotting analysis (Figure 1h). The SEC 4−6 fraction, however, showed strong enrichment of syntenin, whereas calnexin staining was close to the detection

limit in western blot analysis (Figure 1i). TEM analysis showed particles below 200 nm, which portrayed a cup-shape characteristic for EVs (Figure 1j). This indicates that with the sequence of purification methods used we were able to isolate sEVs from human skin.

As an additional approach to test the existence of EVs in human skin, dermal interstitial fluid (dISF) was collected by dermal open flow microperfusion (Bodenlenz et al., 2013) and EVs were enriched by two approaches (Supplementary Figure S1e). After removal of cell debris by centrifugation at 500g and 14,000g, respectively, irregularly shaped, double lipid membrane containing, cup-shaped EVs were visible, similar to those isolated from human skin biopsies (Figure 1k). Nanoparticle tracking analysis of these fractions confirmed a particle median size of around 100 nm (Figure 1l). To increase the purity of the EVs isolated from dISF, we performed SEC and analyzed isolated fractions by TEM. As particle counts were very low in the pooled SEC fractions (Supplementary Figure S1f), we were not able to perform western blot analysis or to capture EVs in fractions 4 to 6. However, in pooled SEC fractions 1 to 3, under omission of the 0.22 μm filtration step, cup-shaped particles with sizes between 50−500 nm were detected, albeit too dilute to capture multiple EVs on single frames because of limited dISF sample material (Figure 1m and Supplementary Figure S1g and h). Still, using immunogold labeling, we confirmed the presence of EV marker protein CD81 on the vesicular membrane of these skin derived EVs (Figure 1m, right image, and Supplementary Figure S1h).

Taken together these data strongly suggest the existence of EVs in the interstitium of the skin, which we were able to visualize and enrich for by using independent sample materials and enrichment strategies.

sEV packaged miRNAs are transferred from fibroblasts to keratinocytes in monolayers and 3D cultures

To confirm an EV-mediated miRNA transfer from HDF to primary normal human epidermal keratinocytes, HDF were transfected with *Caenorhabditis elegans*−specific cel-miR-39, which is packaged into EVs (Hergenreider et al., 2012). The sEVs were isolated from fibroblast supernatants and supplemented to keratinocyte culture media (Figure 2a). Cel-miR-39 was detected in fibroblasts (Figure 2b) and in 2D cultured keratinocytes exposed to the purified sEVs after 48 hours (Figure 2c).

In addition, to further test the transfer of miRNAs from fibroblasts to keratinocytes resembling the epidermis of 3D human skin equivalents, cel-miR-39 transfected fibroblasts were embedded into a collagen matrix ("dermis"; Figure 2a). After full maturation over 10 days, dermis and epidermis were separated, RNA isolated, and cel-miR-39 was confirmed to be still present in the dermis (Figure 2d) and in the epidermis (Figure 2e).

These findings suggest that miRNA cross-talk between fibroblasts and keratinocytes in skin equivalents is not limited by the collagen matrix.

sEVs derived from senescent fibroblasts modulate keratinocyte behavior in vitro

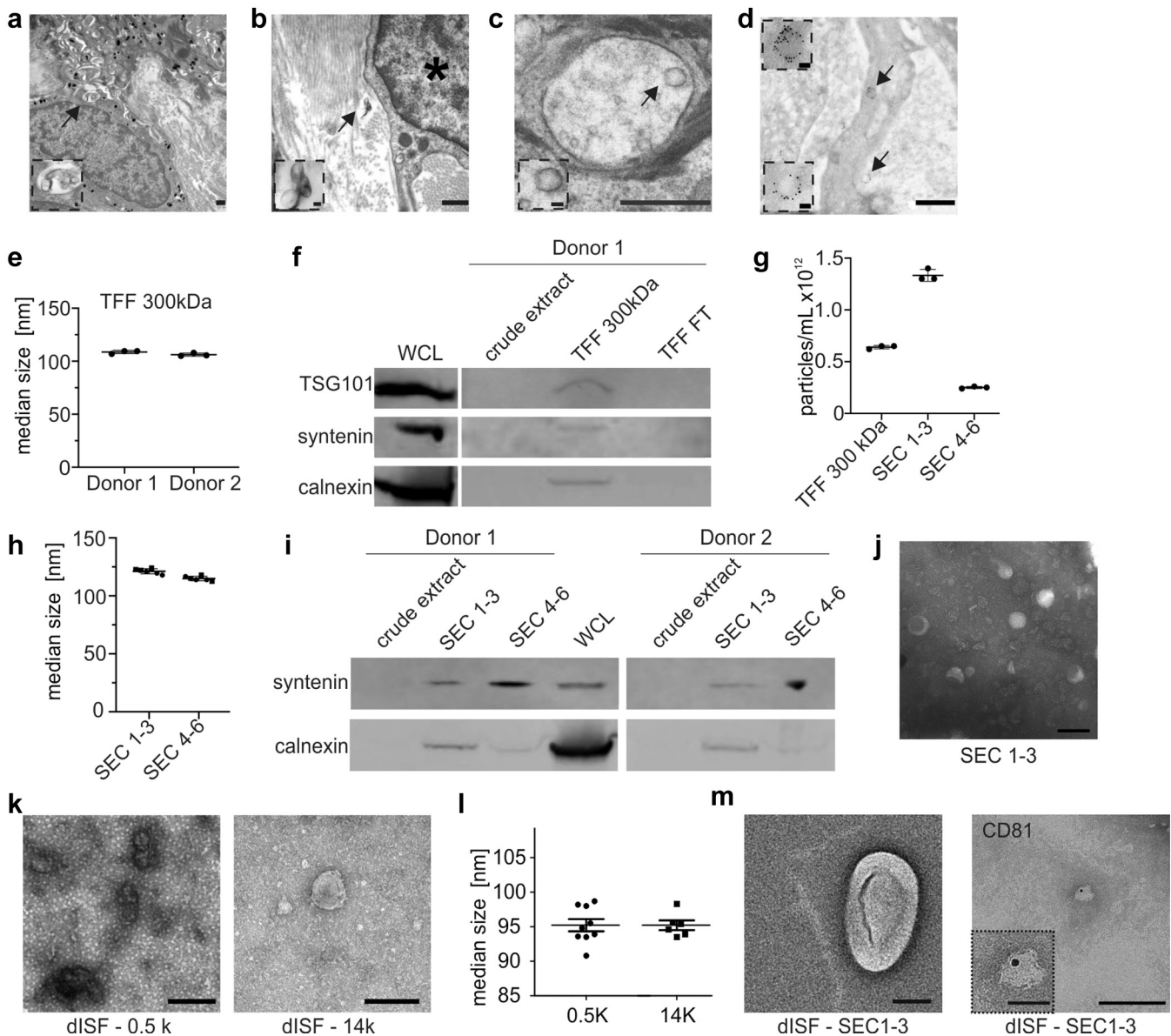Since we recently identified sEVs and their miRNA cargo as, to our knowledge, previously unreported members of the

Figure 1. EVs are present in human skin. (a–d) Skin sections derived from 4 donors were used to detect EV-like structures in human skin by TEM. Scale bar = 500 nm (large image) and 50 nm (region of interest). In (b) a fibroblast cell is marked by *. (a) MVBs and EVs within fibroblasts that are secreted or taken up into/from the extracellular space. Arrow indicates one example MVB. (b) Individual EVs in the collagen matrix (arrow). (c) MVB containing intraluminal vesicles (arrow) in cells of the basal layer. (d) Immunogold labeled ultra-thin cryo-cut skin sections show positive staining for EV-specific protein CD63 on EVs (arrow). (e) NTA of sEVs from human skin sections of 2 donors measured in triplicates. sEVs enriched from the crude extract by TFF with a cut-off of 300 kDa show a median size of approximately 100 nm. (f) Western blots for expression of EV-specific protein TSG101 and syntenin, as well as non-EV protein calnexin. sEVs were enriched after TFF (cut-off of 300 kDa) of crude extract of human skin sections. Whole cell lysate (WCL) of fibroblasts served as positive control, the TFF flow through as negative control. (g) Enriched sEVs from f were further purified using SEC. The first 6 fractions were pooled into 2 samples (SEC 1–3 and SEC 4–6) and subsequently concentrated by spin-filters. NTA measurements reveal high particle count in the first 6 eluted fractions after SEC. (h) NTA of sEVs from g reveals a median size of approximately 121 nm in pooled fractions 1–3 and 114 nm in pooled fractions 4–6. Each donor (●,■) was measured in triplicates. (i) Western blot for expression of EV-specific protein syntenin and non-EV protein calnexin in crude extracts and pooled SEC fractions from g reveals enrichment of EVs in section 4–6. WCL of fibroblasts served as a positive control. (j) TEM image of purified sEVs from g (1:10 dilution of fractions 1–3) reveals particles below 200 nm with a cup-shaped morphology, indicative of sEVs. Scale bar = 200 nm. (k) dISF from 2 donors collected at two positions was centrifuged at 500*g* (0.5K) and subsequently at 14,000*g* (14K). TEM images of both fractions show cup-shaped EVs with a double lipid membrane and sizes between 50 to 150 nm. Scale bar = 200 nm. (l) NTA of the 0.5K and 14K EV fraction from k reveals a median size of 95 nm. 0.5K fractions were measured in technical triplicates. 14K fractions were measured in duplicates. (m) After two centrifugations steps (700*g* and 2,000*g*) EVs from dISF of 2 different donors were further purified by SEC and spin-filters. TEM of pooled fractions 1–3 without (left image) or with (right image) immunogold labeling against tetraspanin CD81. Scale bar = 200 nm (large images) and 50 nm (region of interest). dISF, dermal interstitial fluid; EV, extracellular vesicle; MVB, multivesicular bodies; NTA, nanoparticle tracking analysis; SEC, size exclusion chromatography; sEV, small extracellular vesicle; TEM, transmission electron microscopy; TFF, tangential flow filtration; WCL, whole cell lysate.
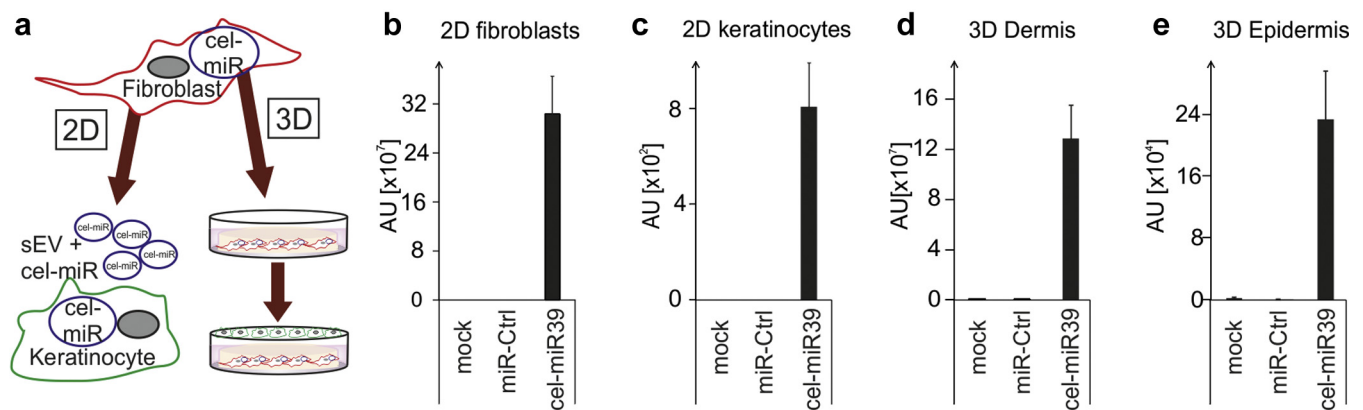
Figure 2. Extracellular vesicles and their miRNA cargo cross-talk between dermal and epidermal cells in monolayers and in 3D full thickness HSE. (a) Experimental design. Cel-miR-39 and a non-targeting control miRNA (miR-Ctrl) were overexpressed in HDF. 24 hours post transfection sEVs were harvested and added to NHEK medium for testing miRNA uptake (2D; left arm). Alternatively (3D; right arm), HDF were embedded into a collagen matrix to build 3D HSE. NHEK were seeded on top and functional HSE were formed in submerse followed by air-liquid interface cultivation. After 10 days, dermis and epidermis were harvested separately, RNA was isolated, and QPCR was performed. (**b**) 24 hours post transfection cel-miR-39 expression in HDF was evaluated by QPCR. (**c**) 48 hours post sEV-incubation, transfer of cel-miR-39 by fibroblast derived sEVs to keratinocytes was evaluated by QPCR. (**d**) 10 days post transfection cel-miR-39 expression was quantified in the dermis of HSE. (**e**) 10 days post transfection cel-miR-39 expression was quantified in the epidermis of HSE. Experiments were performed with fibroblasts and keratinocytes from three different donors. Data are shown as mean ± SEM. For QPCR quantification, raw Ct values were transformed to arbitrary units (AU) by assuming a Ct value of 40 to be 10 AU. HDF, human dermal fibroblast; HSE, human skin equivalent; NHEK, normal human epidermal keratinocytes; QPCR, quantitative reverse transcriptase in real time; SEM, standard error of the mean; sEV, small extracellular vesicle.

senescence-associated secretory phenotype (EV-SASP) of fibroblasts (Terlecki-Zaniewicz et al., 2018), we aimed to test how these sEVs might alter the normal homeostasis of primary keratinocytes. Therefore, HDF were driven into stress-induced premature senescence (SIPS) by repetitive exposure to H_2O_2 (Lämmermann et al., 2018; Terlecki-Zaniewicz et al., 2018). Induction of SIPS was confirmed by increased p21 levels (Supplementary Figure S2a), irreversible growth arrest (not shown), by a flattened and enlarged morphology (Supplementary Figure S2b), and by an increase in SA-ß-Gal activity (Supplementary Figure S2c and d). sEVs of senescent (SIPS) and quiescent control HDF were purified from conditioned media using differential centrifugation and analyzed by TEM (Figure 3a), nanoparticle tracking analysis (Figure 3b), and immunoblotting (Figure 3c). Membranous particles of around 110 nm in size were revealed, which stained positive for the EV-specific marker syntenin and TSG101, but negative for non-EV marker calnexin in western blots.

To monitor how the transient presence of senescent fibroblast derived sEVs modulates wound closure of keratinocytes in vitro, we used a 2D culture model to follow the dynamics of wound closure in terms of repopulation of the cell-free area (gap), as well as using scratch assays after a single addition of sEVs. Keratinocytes of three different donors were exposed for 48 hours to sEVs from quiescent or senescent fibroblasts. Exposure to the senescent cell derived sEVs doubled the number of cells in the cell-free area (Figure 3d and e, and Supplementary Figure S3a) and accelerated the closure dynamics in both assay setups compared with cells exposed to sEVs from quiescent fibroblasts (Figure 3f and Supplementary Figure S3b). Although we cannot differentiate between cell migration and proliferation in our experimental setup, appearance of filopodia and lamellipodia-like protrusions (Figure 3d and Supplementary Figure S3a) and an increase in vimentin expression upon exposure to senescent cell derived sEVs (Figure 3g) point toward an at least partial

contribution by migration, for which a more mesenchymal-like phenotype is a prerequisite (Yan et al., 2010).

In order to test the impact of chronic presence of the EV-SASP on keratinocyte differentiation in vitro, we exposed keratinocytes to sEVs from quiescent or senescent fibroblasts for one week. The presence of senescent cell derived sEVs changed the morphology of the confluent keratinocyte layer (Figure 3h) and reduced the expression levels of the late differentiation marker involucrin (Figure 3i), which is reported to be a main initiator of the cornification process in vivo (Robinson et al., 1996; Watt and Green, 1981).

To summarize, we observed an enhanced scratch/gap (wound) closure with a concomitant rise in vimentin expression after the short term presence of senescent derived sEVs, whereas their chronic presence affected terminal differentiation of keratinocytes in vitro.

miR-23a-3p contributes to the sEV-SASP mediated acceleration of wound closure

In order to test if imbalanced keratinocyte homeostasis might be attributable to specific miRNAs, we selected miR-23a-3p as a prominent candidate because it was highly secreted in sEVs of senescent fibroblasts (Terlecki-Zaniewicz et al., 2018) and repeatedly connected with cellular senescence and skin aging (Röck et al., 2015). Indeed, we confirmed secreted miR-23a-3p to be more abundantly secreted by senescent cells (Supplementary Figure S3c). RNAse digestion in the absence of Triton X-100 was then used to determine miR-23a-3p levels presumably protected by lipid membrane structures (Figure 4a). The fraction of miR-23a-3p that is not accessible to RNAse is still elevated in the sEV preparation of senescent cell supernatants, whereas almost all miR-23a-3p is digested by RNAse treatment in the presence of Triton X-100. This suggests that the vast majority of miR-23a-3p is either freely accessible to RNAse or protected by lipid membranes. The remaining small fraction, which is below
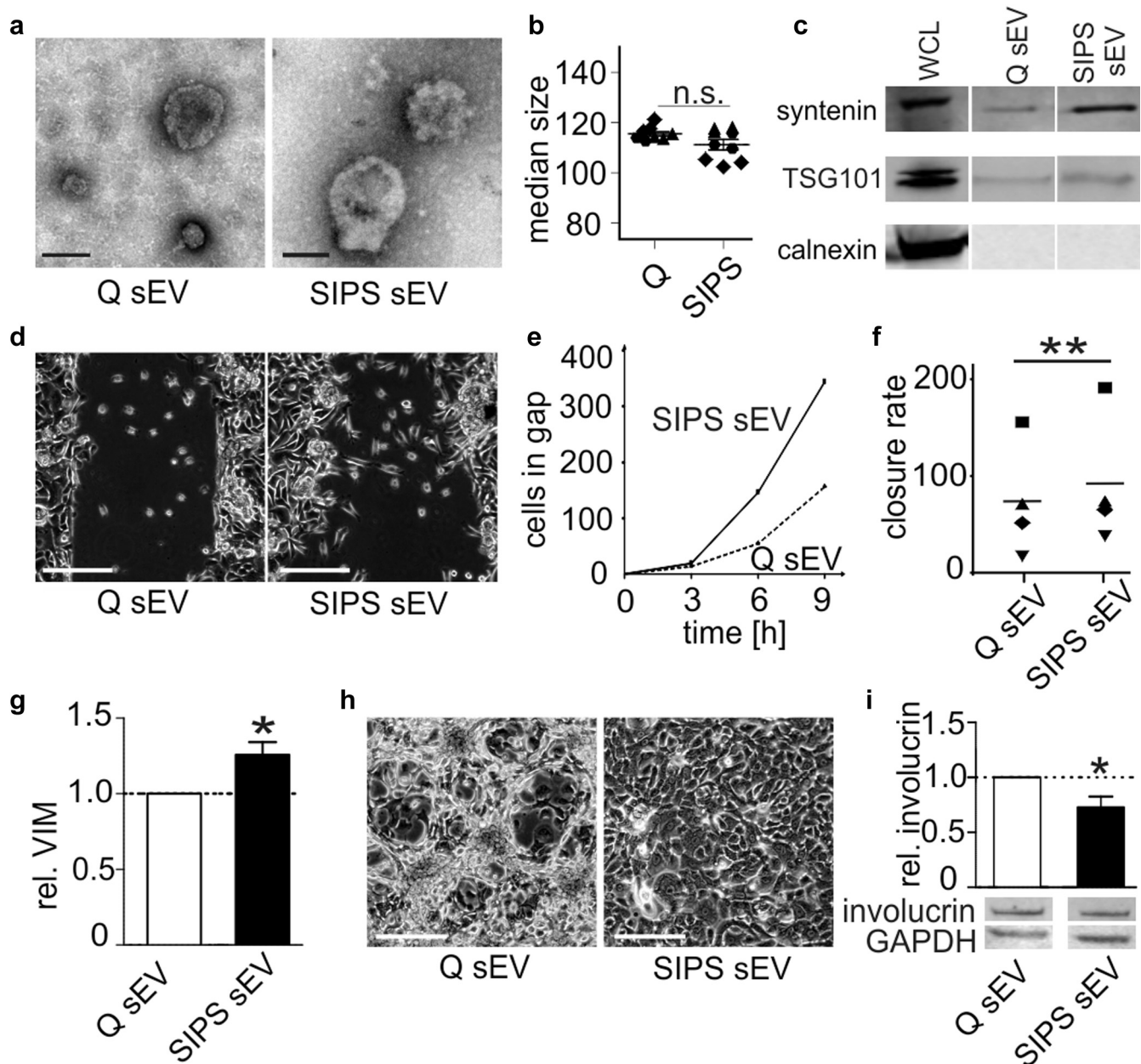
Figure 3. sEVs derived from senescent HDF modulate gap/scratch "wound" closure and differentiation of recipient keratinocytes in vitro. (**a**) Representative transmission electron microscopy image of sEVs purified by differential centrifugation from Q and SIPS HDF. Scale bar = 100 nm. (**b**) Median diameter (×50, [nm]) of sEVs isolated by differential centrifugation. Values (×50) from peak analysis are indicated as mean ± SEM. Samples were measured in technical triplicates from three biological replicates. $P > 0.05$; unpaired Student t test. (**c**) Qualitative western blots for expression of EV-specific proteins TSG101 (44 kDa), syntenin (32 kDa), and non-EV specific protein calnexin (75 kDa) of sEV lysates isolated from conditioned media of quiescent (Q sEV) and senescent (SIPS sEV) fibroblasts by differential centrifugation. Total cell lysate (WCL) of fibroblasts (TSG101) or Hela cells (syntenin, calnexin) served as a control. (**d**) Representative images of keratinocytes growing into cell-free area of 2D culture dishes 9 hours post removal of the inserts. Cells were either exposed to sEVs derived from SIPS or Q HDF for 48 hours. Scale bar = 400 µm. (**e**) Number of keratinocytes within the gap of 2D culture dishes after transient (48 hours) exposure to Q or SIPS derived sEVs at various timepoints. One representative experiment is shown. (**f**) Closure rate of keratinocytes after transient (48 hours) exposure to Q or SIPS derived sEVs was calculated from first and last timepoint as assessed in 2D culture dishes. Dot plot shows single replicates and means from four independent experiments. sEV are derived from three different fibroblast strains (SIPS and Q) and were incubated with keratinocytes of two different donors. **$P < 0.01$; paired Student t test. (**g**) Relative VIM expression after transient (48 hours) exposure to SIPS or Q derived sEVs from HDF. FC ± relative SEM from six independent experiments were calculated after normalization to B2M. *$P < 0.05$; one sample t test. (**h**) Representative images show morphological changes of keratinocytes after chronic exposure (1 week) to SIPS and Q derived sEVs from HDF. Scale bar = 400 µm. (**i**) Representative western blot images of GAPDH and involucrin protein levels. Densiometric analysis of relative involucrin levels normalized to cells exposed to Q sEVs are shown. Averages ± relative SEM from eight independent experiments from three different fibroblast strains and keratinocytes are shown. *$P < 0.05$; Wilcoxon signed rank test. EV, extracellular vesicle; FC, fold change; GAPDH, glyceraldehyde-3-phosphate dehydrogenase; HDF, human dermal fibroblast; n.s., not significant; Q, quiescent; SEM, standard error of the mean; sEV, small extracellular vesicle; SIPS, stress-induced premature senescence/senescent; VIM, vimentin.
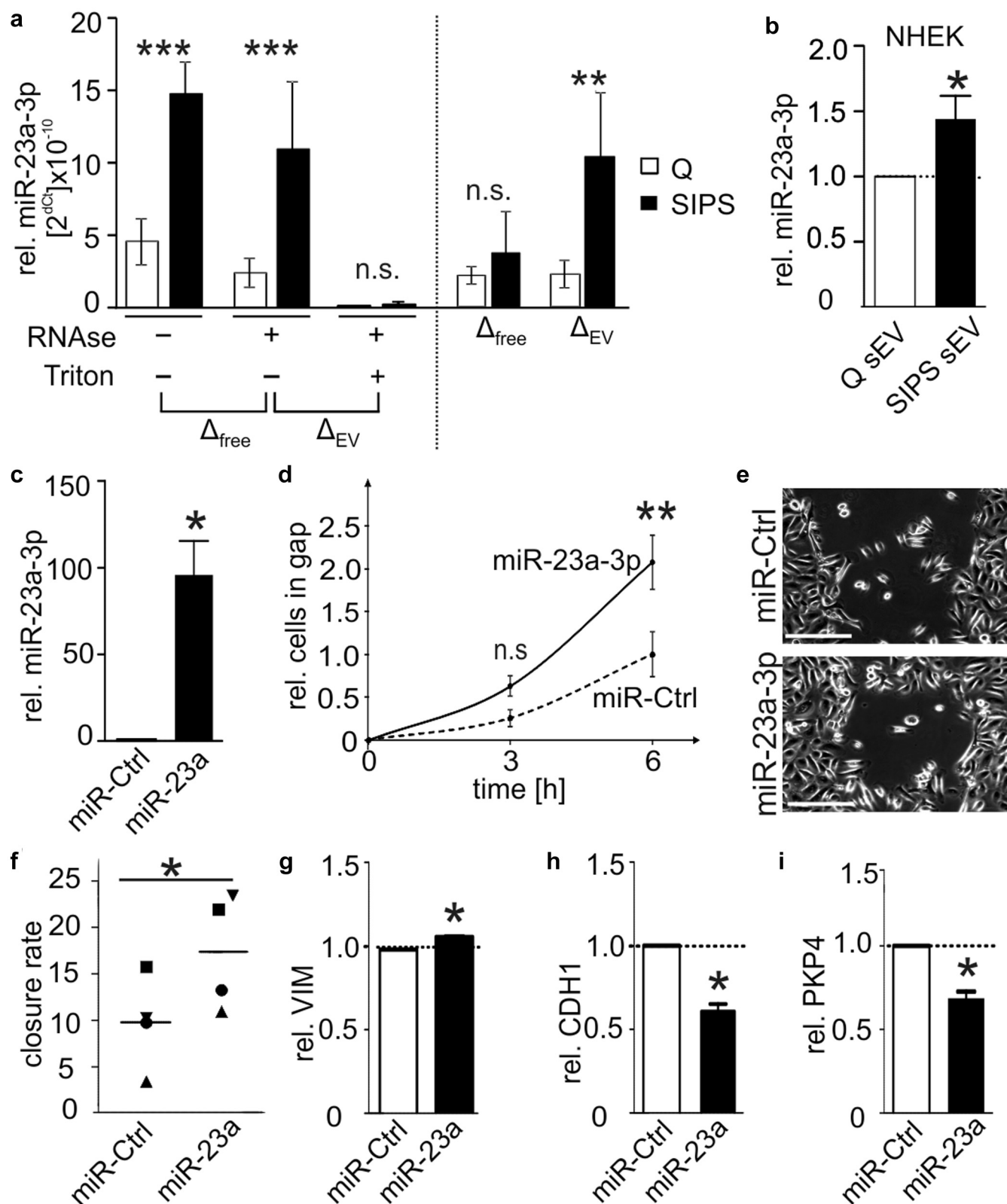
Figure 4. miR-23a-3p phenocopies the effect of senescent cell derived sEVs on wound closure. (**a**) After differential centrifugation, each sample was split into three equal parts, which were treated either with RNAse and Triton X-100 (+/+), RNAse only (+/−), or with HEPES only (−/−). MiR-23a-3p levels were measured by QPCR and normalized to spike-in control and cell count. The amount of free miR-23a-3p (Δ_{free}) is calculated by subtraction of (+/−) signal from (−/−) signal; vesicular miR-23a-3p (Δ_{EV}) by subtraction of (+/+) from (+/−). Data from three independent experiments are shown. Statistical analysis was performed using two-way randomized ANOVA tested for the factor "treatment" ($P < 0.001$) and "SIPS versus Q" ($P < 0.001$), or "Δ_{free} versus Δ_{EV}" ($P = 0.06$) and "SIPS versus Q" ($P = 0.014$). Bonferroni post hoc text was performed to compare individual samples. *$P > 0.05$, **$P < 0.01$, ***$P > 0.001$. (**b**) miR-23a-3p expression in keratinocytes exposed to senescent or quiescent derived sEVs was normalized to U6 as a housekeeper. FC relative to cells exposed to Q derived sEVs were calculated. Mean ± SEM values derived from 11 independent experiments using three different keratinocyte and fibroblast donors. *$P < 0.05$;

7% of the total quantitative reverse transcriptase in real time signal, might be protected by other structures, such as proteinaceous particles.

In order to visualize the influence of senescence on freely accessible (Δ_{free}) versus lipid membrane protected miR-23a-3p (Δ_{EV}), we calculated the respective differences (Figure 4a). Indeed, Δ_{EV} increases significantly in senescent versus control cells, while Δ_{free} miR-23a-3p does not. This indicates that the increase of total miR-23a-3p in the sEV preparations of senescent cells is indeed because of an increased EV-based secretion of this miRNA.

Then, keratinocytes were exposed to sEVs derived from senescent HDF for 48 hours, which resulted in a significant increase of intracellular miR-23a-3p levels (Figure 4b). This, in combination with the transfer of cel-miR-39 from fibroblasts to keratinocytes shown above, suggests an uptake of this miRNA via sEVs by keratinocytes in vitro. However, we have not excluded whether miR-23a-3p might be induced endogenously after sEV exposure within keratinocytes.

To investigate if miR-23a-3p might contribute to the accelerated scratch and gap (wound) closure seen by senescent cell derived sEVs, we transfected keratinocytes with pre-miR-23a-3p and a non-targeting control miRNA. Overexpression was confirmed (Figure 4c) and enhanced gap closure, in terms of cells present in the cell-free area (Figure 4d and e, and Supplementary Figure S3d), as well as closure dynamics (Figure 4f) were observed. In addition, miR-23a-3p transfected cells showed mesenchymal cell-like protrusions (Figure 4e and Supplementary Figure S3d), as it was similarly seen after exposure to senescent cell derived sEVs. In addition, a slight increase in vimentin expression (Figure 4g) and a concomitant decrease of miR-23a-3p's direct target E-cadherin (Cao et al., 2012) were observed (Figure 4h), suggesting again an at least partial epithelial-to-mesenchymal transition. Plakophilin 4 (PKP4/p0071) is a predicted putative target of miR-23a-3p in keratinocytes (Agarwal et al., 2015), which was significantly reduced by miR-23a-3p (Figure 4i). Plakophilin 4A interacts with the desmosomal plaques and the adherens junctions to regulate mechanical strength of keratinocyte monolayers (Calkins et al., 2003). However, miR-23a-3p did not modulate keratinocyte differentiation as assessed by involucrin levels one week after transfection (data not shown).

DISCUSSION

Cross-talk of fibroblasts to keratinocytes by soluble factors affect skin homeostasis, as knockout of AP-1 components in fibroblasts has been shown to impair epidermal differentiation (Szabowski et al., 2000) and wound healing in mouse models in vivo (Florin et al., 2006). However, little is known as to whether EVs and their miRNA cargo exist in different layers of the human skin and if they are involved in the regulation of skin homeostasis during aging. Here we report the presence of multivesicular bodies as one source of secreted sEVs in fibroblasts. This presence of EVs in vivo is supported by indications of EVs at sides of wounds from human skin biopsies (Huang et al., 2015) and their visualization adjacent to interstitial dermal cells by 3D electron microscopy (Cretoiu et al., 2015).

In the context of fibroblast aging, little is known about EVs (Lehmann et al., 2008; Terlecki-Zaniewicz et al., 2018). Cellular senescence is a key driver of the aging process, and the SASP has been shown to promote tumorigenesis of epidermal cells (Krtolica et al., 2001) and to increase the number of senescent keratinocytes re-entering the cell cycle, concomitantly with a partial epithelial-to-mesenchymal transition of these escape-keratinocytes (Malaquin et al., 2013). Senescent cell derived EVs have been reported to confer part of this pro-tumorigenic activity (Takasugi et al., 2017), which might be partly attributable to increased secretion of senescent fibroblasts derived EVs (Lehmann et al., 2008) and/or to changes in their miRNA composition (Terlecki-Zaniewicz et al., 2018).

Intriguingly, our data suggest that senescent cell derived sEVs accelerate the scratch/gap closure of keratinocytes in vitro. This is in line with in vivo data showing enhanced wound healing (Demaria et al., 2014) and tissue regeneration (Ritschka et al., 2017) as a beneficial and elementary characteristic of the transient presence of senescent cells and the SASP. However, impaired removal of senescent cells because of decreased immunosurveillance and a constrained T-cell mobility through the extracellular matrix (Moreau et al., 2017) or because of accumulation of senescence by intrinsic or extrinsic stressors leads to chronic accumulation of senescent cells in the skin (Herbig et al., 2006; Lewis et al., 2011). This chronic presence of senescent cells and the SASP might impair tissue homeostasis leading to a gradual loss of barrier function and juvenile appearance, skin malignancies, and to an impaired fibroblasts contraction in wounds (Ballas and Davidson, 2001).

This is in accordance with a restrained epidermal differentiation, which was observed after chronic exposure to sEVs from senescent fibroblasts, substantiating the double-edged role of the SASP and its members, the sEVs. Considering the fine tuning capacity of EV-miRNAs during normal skin homeostasis (Lo Cicero et al., 2015) and their differential

secretion during senescence, we speculate that SASP-miRNAs of fibroblasts (Terlecki-Zaniewicz et al., 2018) affect normal keratinocyte homeostasis, as it was similarly shown for endothelial senescence-associated EV-miR-31 in the context of osteogenic differentiation (Weilner et al., 2016). Indeed, we identified miR-23a-3p, highly secreted from senescent fibroblasts, as a crucial mediator of the wound healing mediated effect induced by the EV-SASP.

miR-23a-3p is well connected to transforming growth factor ß—induced epithelial-to-mesenchymal transition (Cao et al., 2012), cellular senescence (Guo et al., 2013; Markopoulos et al., 2017), and skin aging (Dreesen et al., 2013), showing an age dependent increase in skin sections of old mice and in fibroblasts derived from elderly donors (Röck et al., 2015). Known targets of miR-23a-3p include hyaluronan synthase 2 and E-cadherin, linking it to extracellular matrix production, cardiac development, and tumor progression (Bernert et al., 2011; Camenisch et al., 2001; Cao et al., 2012; Ma et al., 2017). In addition, the predicted target PKP4/p0071 was significantly reduced in keratinocytes upon miR-23a-3p overexpression. It directly interacts with E-cadherin reducing its activity (Keil et al., 2013) and mediates the fine tuning between desmosomal plaques and adherens junctions, in order to regulate mechanical strength versus cell migration (Calkins et al., 2003). Our data support this idea, since increased levels of E-cadherin confer an inhibitory effect on wound healing of epithelial cells (Setzer et al., 2004).

To conclude, we here unraveled the ubiquitous presence of EVs in human skin and their ability to deliver their miRNA cargo from fibroblasts through the collagen matrix into the epidermal layer of 3D human skin equivalents. Finally, we identified fibroblast derived vesicular miR-23a-3p as a crucial "miR-diator" of the EV-SASP induced acceleration of scratch/gap closure in keratinocytes in vitro.

Thus, we are confident that the presence of EVs and their miRNA cargo contributes to the development and recurrence of cutaneous lesions during age-associated diseases and emphasize the necessity to further investigate their functional role.

MATERIAL AND METHODS

Human skin samples
All cells and tissues are derived post liposuction from healthy adult female subjects in the age range of 30 to 40 years. The study was approved by the ethics committee of the Medical University of Vienna and was conducted in accordance with the principles of the Declaration of Helsinki. Written informed consent was obtained (vote no. 1149/2011).

Dermal open flow microperfusion
Human skin samples were used to collect dISF by dermal open flow microperfusion (Bodenlenz et al., 2013). The skin samples were obtained during plastic surgery and were provided by Biobank Graz, Austria, after approval of the ethics committee of the Medical University of Graz (vote no, 28-151 ex 15/16).

Three dermal probes were inserted into each skin sample at different locations immediately after excision. The probes were continuously perfused with physiological saline solution at a flow rate of 1 µl/min in a push-pull manner using a OFM pump (Joanneum Research, Austria). dISF samples were collected at room temperature in one-hour intervals. After each interval, the dISF samples were stored at 4 °C until the isolation of EVs and further TEM measurements and nanoparticle tracking analysis.

Cell culture
All cells were regularly tested for mycoplasma. They were cultivated at 95% air humidity, 7% CO2, and at 37 °C.

Primary HDF from adult human skin of three healthy donors were acquired from Evercyte GmbH (Vienna, Austria). Cells were cultivated in DMEM/Ham's F-12 (1:1 mixture; Biochrom, Berlin, Germany) supplemented with 10% fetal calf serum and 4 mM L-Glutamine (Sigma-Aldrich GmbH, St Louis, MO, USA). Cells were passaged twice a week at a split ratio of 1:2.

Normal human epidermal keratinocytes from adult human skin of three health donors were acquired from Evercyte GmbH. Cells were grown in Dermalife K media supplemented with Dermalife K Life-Factors kit (LifeLine Cell Technology, Frederick, MD). Cells were regularly thawed in passage 2/PD2.5, passaged once in a split ratio of 1:4, and used upon confluence for subsequent experiments.

Stress-induced premature senescence
For induction of SIPS, HDF derived from three different donors were seeded at 3500 cells/cm^2 24 hours before stress treatment. Cells were treated with nine doses of 80 µM H_2O_2 for 1 hour per day followed by a media change (4 days stress, 2 days recovery, 5 days stress). Control cells were mock-treated and reached quiescence by contact inhibition. Induction of SIPS was confirmed earlier (Terlecki-Zaniewicz et al., 2018) by SA-ß-Gal staining, CDKN1A (p21) expression, and by prominent morphological changes.

Full thickness human skin equivalents
Human skin equivalents were generated as published earlier (Mildner et al., 2006). A detailed protocol can be found in the supplementary material.

Culture insert for gap (wound) closure and scratch assay

Culture inserts to monitor gap closure. Keratinocytes were seeded with 3 × 10^4 cells/cm^2 into µ-Dish 35 wound healing chambers containing culture inserts (IBIDI, Martinsried, Germany). Twenty-four hours after seeding, sEVs were added, and upon confluence (24—48 hours incubation), the silicone insert was removed leaving behind a cell-free area (gap = wound). Fresh culture media was added, and cells were incubated at 37 °C at 7% CO$_2$.

Scratch assay. Keratinocytes were seeded into 12-well plates. Upon confluence, the monolayer was scratched using a 200 µl pipette tip. Gap closure was monitored by capturing non-overlapping images along the entirety of the gap/scratch every 3 hours. For the culture inserts, number of cells within the cell-free area were counted manually in a blinded fashion. Scratch assays were quantified using the freehand line tool measuring the entire scratch area. For both assays, the wound closure rate ("slope") per hour was calculated as shown below.

$$(\text{area or cells } t_{n+1} - \text{ area or cells } t_0) \div (t_{n+1} - t_0)$$

Isolation of small extracellular vesicles
EV purification was performed according to standards recommended from the international society for extracellular vesicles (Hill et al., 2013).

From conditioned media of HDF. Fetal calf serum containing media was depleted from EVs by ultracentrifugation at 100,000g overnight and filtrated using 0.22 μm filter cups (Millipore, Darmstadt, Germany). Cells were allowed to secrete for 48 hours. Differential centrifugation was performed at 4 °C. Conditioned media was centrifuged at 500g (5804R; Eppendorf, Hamburg, Germany) for 15 minutes to exclude cellular debris, followed by centrifugation at 14,000g (Avanti JXN-26; Beckmann Coulter, Brea, CA) for 15 minutes. Large EVs were removed by filtration using 0.22 μm filter cups and supernatant was filled into Quick-Seal, Polyallomer, 39 ml, 25 × 89 mm tubes (Beckmann Coulter) to enrich sEVs at 100,000g for 90 minutes using a 70Ti Rotor (Beckmann Coulter). For subsequent analysis, the pellet was resuspended in filtered phosphate buffered saline (PBS) or keratinocyte media. For functional assays and TEM, freezing and thawing were avoided. The amount of vesicles used for keratinocyte exposure was quantified by the number of secreting fibroblasts to the number of receiving keratinocytes. For functional studies, sEVs in a ratio of 5:1 (fibroblasts:keratinocytes) were used.

From skin sections. Adipose tissue of two skin sections was removed and tissue sections consisting of dermis and epidermis were disintegrated using 1.5 U dispase at 4 °C overnight with continuous agitation followed by incubation at 37 °C for 3 hours. Accessible soluble material was collected and pooled with filtered PBS that was used to wash skin sections twice (crude extract). Subsequently, the crude extract was used for sEV isolation by differential centrifugation followed by filtration using 0.45 μm and 0.22 μm syringe filters. Finally, sEVs were enriched by tangential flow filtration with a cut-off of 300 kDa (mPES MicroKros Filter Modules 300 kD, C02-E300-05-N; Spectrum Labs, Rancho Dominguez, CA) to 1 ml. During this process, flow through was collected. The retentate was then diafiltrated twice using the same system with 15 ml 0.22 μm-filtered PBS. The retentate was then either analyzed as it was or further purified by SEC (see below).

From dermal interstitial fluid. The dISF samples of the first 2 hours were pooled and filled up to 200 μL with 10 mM HEPES buffer and centrifuged at 500g for 15 minutes (0.5k fraction). Supernatant was collected and further centrifuged at 14,000g for 15 minutes (14k fraction). Both fractions were used for TEM and nanoparticle tracking analysis. To achieve a greater purity, in a different setup dISF samples from 1-, 2-, and 3-hour timepoints of open flow microperfusion from two donors were pooled and filled up to 500 μL with 0.22 μm-filtered PBS. Samples were centrifuged at 500g for 5 minutes, supernatants collected and centrifuged again at 2,000g for 10 minutes. Supernatants were then applied to SEC columns (see below).

Size exclusion chromatography. SEC was used to achieve greater purity of EVs isolated from skin sections and dISF. We used qEV original columns (70 nm; IZON Science, Christchurch, New Zealand) according to the manufacturer's instructions. Briefly, approximately 500 μL of sample were applied on the column and after 3 ml of void volume, 22 fractions of approximately 0.5 ml each were collected. As according to the manufacturer, the first six fractions contain the bulk of EVs, we pooled fractions 1 to 3 and 4 to 6, and further concentrated them using Amicon spin-filters (10 kDa) until 1.5 ml sample were concentrated to ∼30−50 μL. These were then used for subsequent analysis.

RNAse and Triton X-100 treatment of isolated sEVs

sEVs were isolated from conditioned media of either quiescent or SIPS HDF according to the aforementioned protocol (see above). Each sample was split into three equal parts and treated either with the following: (i) 38 μg/ml RNAse (+/−, EN0531; Thermo Fisher Scientific, Waltham, MA); (ii) 38 μg/ml RNAse + 1% Triton X-100 (+/+); or (iii) equivalent amounts of 10 mM HEPES (−/−). After incubation at 37 °C for 30 minutes, samples were mixed with five times the original volume in QIAzol Lysis Reagent (79306; QIAGEN, Hilden, Germany) and 1 μL spike-in mix containing UniSp2, UniSp4, and UniSp5 (203203; Exiqon, Vedbaek, Denmark). MiR23a-3p Ct values were normalized to spike-in control (UniSp2) and cell count. Free miR-23a-3p levels were calculated by subtraction of (+/−) signals from (−/−) signals. Subtraction of (+/+) levels from (+/−) levels yielded the amount of vesicular miR-23a-3p.

Transmission electron microscopy

For TEM measurements two different protocols were used.

In one protocol (Figure 1k, left picture, and Figure 3a), solutions used for the staining procedure were prefiltered using 0.22 μm filter units. Athene Old 300 mesh copper grids (Agar Scientific, Stansted, Essex, United Kingdom) were used to adhere sEVs isolated from conditioned media or dISF. The sample was fixed with 1% glutaraldehyde, washed 3 times with nuclease free water, and sEVs were stained for 5 minutes with 2% phosphotungstic acid hydrate (Carl Roth, Karlsruhe, Germany). The grids were left to dry and the specimens were visualized using TEM (FEI Tecnai T20, FEI Eindhoven, Netherlands) operated at 160 kV.

In the second protocol (all other TEM images: Figure 1a−c, j, m), 5 μl of sample were added to glow-discharged Formvar-carbon type B coated electron microscopy grids for 3 minutes, after which the sample was removed by using wet Whatman filter paper. Grids were either prepared for immunogold labeling (see below) or carefully washed twice with filtered PBS before 5 μL of filtered 2% uranyl acetate were added for 10−30 seconds. Then, uranyl acetate was removed using wet Whatman filter paper, and grids were air dried for 2 minutes and imaged.

For immunogold labeling, grids were blocked after the initial binding step of the sample using filtered 2% BSA (in PBS) for 10 minutes. After blocking, grids were placed on 15 μL primary antibody solution (anti-CD81 1:50 in 0.2% BSA) for 60 minutes. Post incubation, grids were washed with 0.2% BSA six times and afterwards placed on a goat anti-mouse secondary antibody solution containing 10 nm gold particles (dilution 1:50) for 60 minutes. Post incubation, grids were washed six times with PBS followed by six washing steps with ddH$_2$O. Finally, grids were placed on 0.2% uranyl acetate for 10 to 30 seconds. Uranyl acetate was removed using a wet Whatman filter paper, and grids were air dried for 2 minutes and imaged.

TEM of resin embedded skin sections. All specimens were fixed in a buffered 3% glutaraldehyde solution, postfixed in osmium tetroxide (3%) for 2 hours, dehydrated through a graded acetone series, and embedded in Araldite (Fluka, Buchs, Switzerland). Ultrathin sections (60−90 nm thickness) were prepared using a diamond knife, collected on copper grids (G 300 Cu), and examined with a Jeol JEM-1400 Plus electron microscope.

Immunolabeling of resin-free ultrathin cryo-cut sections. Human skin biopsies were fixed in 2% paraformaldehyde and 0.2%

glutaraldehyde (both from EMS, Hatfield, USA) in 0.1 M PHEM buffer pH 6.9 for 2 hours at room temperature, then over night at 4 °C. Samples were cut into 1 mm³ blocks that were immersed in 2.3 M sucrose for 1 week at 4 °C. These blocks were mounted onto Leica specimen carrier (Leica Microsystems, Vienna, Austria) and frozen in liquid nitrogen. With a Leica UCT/ fetal calf serum cryo-ultramicrotome (Leica Microsystems, Vienna, Austria) the frozen blocks were cut into ultrathin sections at a nominal thickness of 60 nm at −120 °C. A mixture of 2% methylcellulose and 2.3 M sucrose in a ratio of 1:1 was used as a pickup solution. Sections were picked up onto 200 mesh Ni grids (Gilder Grids, Lincolnshire, United Kingdom) with a carbon coated Formvar film (Fixation, embedding, and cryo-sectioning as described by Tokuyasu, 1973).

Before immunolabeling, grids were placed on plates with solidified 2% gelatin and warmed up to 37 °C for 20 minutes to remove the pickup solution. After quenching of free aldehyde-groups with glycine (0.1% for 15 minutes), a blocking step with 1% BSA (fraction V) in 0.1M Sörensen phosphate buffer pH 7.4 was performed for 30 minutes. The grids were incubated in primary antibody, mouse anti-CD63 (ab8219; Abcam, Cambridge, United Kingdom), diluted 1:1000 in 0.1 M Sörensen phosphate buffer containing 0.1% BSA (Fraction V) overnight at 4 °C, followed by a 2-hour incubation in the secondary antibody, a goat-anti-mouse antibody coupled with 6 nm gold (GAR 6 nm, Aurion, Wageningen, The Netherlands), diluted 1:20 in 0.1 M Sörensen phosphate buffer containing 0.1% BSA (Fraction V), performed at room temperature. The sections were stained with 4% uranyl acetate (Merck, Darmstadt, Germany) and 2% methylcellulose in a ratio of 1:9 (on ice). All labeling steps were done in a wet chamber. The sections were inspected in a FEI Morgagni 268D TEM (FEI, Eindhoven, The Netherlands) operated at 80 kV. Electron micrographs were acquired using an 11 megapixel Morada CCD camera from Olympus-SIS (Münster, Germany).

Statistical analysis
Routine statistics were either calculated with Excel or Graph Pad Prism, version 5.03, and respective tests are indicated in figure legends. Averages from at least three independent experiments with different cell strains are presented as mean ± standard error of the mean or standard deviation. Two-tailed *t* tests were performed using an error probability of 0.05.

Data was tested for Gaussian distribution using the Shapiro-Wilk test. If normal distributed, two groups were compared using unpaired or paired Student *t* test using raw values. One sample Student *t* test or Wilcoxon signed rank test was used to compare ratios to a hypothetical value of 1 after normalization. Comparison of more than two groups was performed using one-way analysis of variance after Tukey's multiple comparison tests. To analyze the impact of two independent factors a two-way repeated measure analysis of variance was performed followed by Bonferroni post test.

Additional information on the material and methods are available in the supplementary text.

Data availability statement
Datasets related to this article are available from the corresponding author upon reasonable request.

ORCIDs
Lucia, Terlecki-Zaniewicz: https://orcid.org/0000-0003-2243-9869
Vera, Pils: https://orcid.org/0000-0002-3794-0376
Madhusudhan Reddy, Bobbili: https://orcid.org/0000-0001-9955-0675
Ingo, Lämmermann: https://orcid.org/0000-0001-6675-0734
Ida, Perrotta: https://orcid.org/0000-0002-9061-9776
Tonja, Grillenberger: https://orcid.org/0000-0002-4140-041X
Jennifer, Schwestka: https://orcid.org/0000-0001-8824-2159
Katrin, Weiß: https://orcid.org/0000-0002-0189-9885
Dietmar, Pum: https://orcid.org/0000-0002-1895-4940
Elsa, Arcalis: https://orcid.org/0000-0001-9883-465X
Simon, Schwingenschuh: https://orcid.org/0000-0001-9549-1065
Thomas, Birngruber: https://orcid.org/0000-0001-8827-4660
Marlene, Brandstetter: https://orcid.org/0000-0002-8134-4985
Thomas, Heuser: https://orcid.org/0000-0001-7385-0178
Markus, Schosserer: https://orcid.org/0000-0003-2025-0739
Frédérique, Morizot: https://orcid.org/0000-0003-0601-7885
Michael, Mildner: https://orcid.org/0000-0002-6892-925X
Eva, Stoeger: https://orcid.org/0000-0002-7651-7992
Erwin, Tschachler: https://orcid.org/0000-0002-0248-1798
Regina, Weinmüllner: https://orcid.org/0000-0002-3971-4348
Florian, Gruber: https://orcid.org/0000-0003-1094-5641
Johannes, Grillari: https://orcid.org/0000-0001-5474-6332

AUTHOR CONTRIBUTIONS
Conceptualization: LTZ, JG, FG, FM; Data Curation: LTZ, VP, JG, FG, IL, MRB, DP, EA, ES, MB, TH, IP, MS; Formal Analysis: LTZ, VP, DP, EA, ES, IP, MB, TH, MRB, IL; Funding Acquisition: JG, FG; Investigation: LTZ, VP, TG, IP, JS, RW, IL, MRB, MS, KW, SS, TB, MB, EA, DP, TH, MM; Methodology: LTZ, MRB, IL, VP, RW, TB, SS; Project Administration: FG, JG; Resources: TB, SS, MM, ET; Supervision: JG, FG, ET, FM; Validation: MB, TH, EA, DP; Visualization: LTZ, RW, VP, IL, MS, JG; Writing - Original Draft Preparation: LTZ, JG, RW, VP, IL, MRB, MS, FG; Writing - Review and Editing: LTZ, VP, MRB, IL, IP, TG, JS, KW, DP, EA, SS, TB, MB, TH, MS, FM, MM, ES, ET, RW, FG, JG.

SUPPLEMENTARY MATERIAL
Supplementary material is linked to the online version of the paper at www.jidonline.org, and at https://doi.org/10.1016/j.jid.2019.05.015.

REFERENCES
Agarwal V, Bell GW, Nam JW, Bartel DP. Predicting effective microRNA target sites in mammalian mRNAs. Elife 2015;4:e05005.

Baker DJ, Childs BG, Durik M, Wijers ME, Sieben CJ, Zhong J, et al. Naturally occurring p16 Ink4a -positive cells shorten healthy lifespan. Nature 2016;530:184—9.

Ballas CB, Davidson JM. Delayed wound healing in aged rats is associated with increased collagen gel remodeling and contraction by skin fibroblasts, not with differences in apoptotic or myofibroblast cell populations. Wound Repair Regen 2001;9:223—37.

Bernert B, Porsch H, Heldin P. Hyaluronan synthase 2 (HAS2) promotes breast cancer cell invasion by suppression of tissue metalloproteinase inhibitor 1 (TIMP-1). J Biol Chem 2011;286:42349—59.

Bodenlenz M, Aigner B, Dragatin C, Liebenberger L, Zahiragic S, Höfferer C, et al. Clinical applicability of dOFM devices for dermal sampling. Skin Res Technol 2013;19:474—83.

Botchkareva NV. MicroRNA/mRNA regulatory networks in the control of skin development and regeneration. Cell Cycle 2012;11:468—74.

Calkins CC, Hoepner BL, Law CM, Novak MR, Setzer SV, Hatzfeld M, et al. The armadillo family protein p0071 is a VE-cadherin- and desmoplakin-binding protein. J Biol Chem 2003;278:1774—83.

Camenisch TD, Biesterfeldt J, Brehm-Gibson T, Bradley J, McDonald JA. Regulation of cardiac cushion development by hyaluronan. Exp Clin Cardiol 2001;6:4−10.

Cao M, Seike M, Soeno C, Mizutani H, Kitamura K, Minegishi Y, et al. MiR-23a regulates TGF-β-induced epithelial-mesenchymal transition by targeting E-cadherin in lung cancer cells. Int J Oncol 2012;41:869−75.

Coppé JP, Desprez PY, Krtolica A, Campisi J. The senescence-associated secretory phenotype: the dark side of tumor suppression. Annu Rev Pathol 2010;5:99−118.

Cretoiu D, Gherghiceanu M, Hummel E, Zimmermann H, Simionescu O, Popescu LM. FIB-SEM tomography of human skin telocytes and their extracellular vesicles. J Cell Mol Med 2015;19:714−22.

Demaria M, Ohtani N, Youssef SA, Rodier F, Toussaint W, Mitchell JR, et al. An essential role for senescent cells in optimal wound healing through secretion of PDGF-AA. Dev Cell 2014;31:722−33.

Dreesen O, Ong PF, Chojnowski A, Colman A. The contrasting roles of lamin B1 in cellular aging and human disease. Nucleus 2013;4:283−90.

Florin L, Knebel J, Zigrino P, Vonderstrass B, Mauch C, Schorpp-Kistner M, et al. Delayed wound healing and epidermal hyperproliferation in mice lacking JunB in the skin. J Invest Dermatol 2006;126:902−11.

Guo Z, Zhou B, Liu W, Xu Y, Wu D, Yin Z, et al. MiR-23a regulates DNA damage repair and apoptosis in UVB-irradiated HaCaT cells. J Dermatol Sci 2013;69:68−76.

Herbig U, Ferreira M, Condel L, Carey D, Sedivy JM. Cellular senescence in aging primates. Science 2006;311:1257.

Hergenreider E, Heydt S, Tréguer K, Boettger T, Horrevoets AJG, Zeiher AM, et al. Atheroprotective communication between endothelial cells and smooth muscle cells through miRNAs. Nat Cell Biol 2012;14:249−56.

Hill AF, Pegtel DM, Lambertz U, Leonardi T, Driscoll LO, Pluchino S, et al. ISEV position paper: extracellular vesicle RNA analysis and bioinformatics. J Extracell Vesicles 2013;2.

Huang P, Bi J, Owen GR, Chen W, Rokka A, Koivisto L, et al. Keratinocyte microvesicles regulate the expression of multiple genes in dermal fibroblasts. J Invest Dermatol 2015;135:3051−9.

Iraci N, Leonardi T, Gessler F, Vega B, Pluchino S. Focus on extracellular vesicles: physiological role and signalling properties of extracellular membrane vesicles. Int J Mol Sci 2016;17:171.

Jang SC, Crescitelli R, Cvjetkovic A, Belgrano V, Bagge RO, Hoog JL, et al. A subgroup of mitochondrial extracellular vesicles discovered in human melanoma tissues are detectable in patient blood [preprint]. bioRxiv 2017. (accessed 27 June 2019).

Jun JII, Lau LF. Cellular senescence controls fibrosis in wound healing. Aging (Albany NY) 2010;2:627−31.

Keil R, Schulz J, Hatzfeld M. P0071/PKP4, a multifunctional protein coordinating cell adhesion with cytoskeletal organization. Biol Chem 2013;394:1005−17.

Krtolica A, Parrinello S, Lockett S, Desprez PY, Campisi J. Senescent fibroblasts promote epithelial cell growth and tumorigenesis: a link between cancer and aging. Proc Natl Acad Sci U S A 2001;98:12072−7.

Lämmermann I, Terlecki-Zaniewicz L, Weinmüllner R, Schosserer M, Dellago H, de Matos Branco AD, et al. Blocking negative effects of senescence in human skin fibroblasts with a plant extract. NPJ Aging Mech Dis 2018;4:4.

Lehmann BD, Paine MS, Brooks AM, McCubrey JA, Renegar RH, Wang R, et al. Senescence-associated exosome release from human prostate cancer cells. Cancer Res 2008;68:7864−71.

Lewis DA, Travers JB, Machado C, Somani AK, Spandau DF. Reversing the aging stromal phenotype prevents carcinoma initiation. Aging (Albany NY) 2011;3:407−16.

Lo Cicero A, Delevoye C, Gilles-Marsens F, Loew D, Dingli F, Guéré C, et al. Exosomes released by keratinocytes modulate melanocyte pigmentation. Nat Commun 2015;6:7506.

Ma F, Li W, Liu C, Li W, Yu H, Lei B, et al. MiR-23a promotes TGF-β1-induced EMT and tumor metastasis in breast cancer cells by directly targeting CDH1 and activating Wnt/β-catenin signaling. Oncotarget 2017;8:69538−50.

Malaquin N, Vercamer C, Bouali F, Martien S, Deruy E, Wernert N, et al. Senescent fibroblasts enhance early skin carcinogenic events via a paracrine MMP-PAR-1 axis. PLoS ONE 2013;8.

Markopoulos GS, Roupakia E, Tokamani M, Vartholomatos G, Tzavaras T, Hatziapostolou M, et al. Senescence-associated microRNAs target cell cycle regulatory genes in normal human lung fibroblasts. Exp Gerontol 2017;96:110−22.

Merjaneh M, Langlois A, Larochelle S, Cloutier CB, Ricard-Blum S, Moulin VJ. Pro-angiogenic capacities of microvesicles produced by skin wound myofibroblasts. Angiogenesis 2017;20:385−98.

Mildner M, Ballaun C, Stichenwirth M, Bauer R, Gmeiner R, Buchberger M, et al. Gene silencing in a human organotypic skin model. Biochem Biophys Res Commun 2006;348:76−82.

Moreau J-F, Pradeu T, GRignolio A, Nardini C, Castiglione F, Tieri P, et al. The emerging role of ECM crosslinking in T cell mobility as a hallmark of immunosenescence in humans. Ageing Res Rev 2017;35:322−35.

Nakamura K, Jinnin M, Harada M, Kudo H, Nakayama W, Inoue K, et al. Altered expression of CD63 and exosomes in scleroderma dermal fibroblasts. J Dermatol Sci 2016;84:30−9.

Ni C, Narzt MS, Nagelreiter IM, Zhang CF, Larue L, Rossiter H, et al. Autophagy deficient melanocytes display a senescence associated secretory phenotype that includes oxidized lipid mediators. Int J Biochem Cell Biol 2016;81:375−82.

Ressler S, Bartkova J, Niederegger H, Bartek J, Scharffetter-Kochanek K, Jansen-Dürr P, et al. p16INK4A is a robust in vivo biomarker of cellular aging in human skin. Aging Cell 2006;5:379−89.

Ritschka B, Storer M, Mas A, Heinzmann F, Ortells MC, Morton JP, et al. The senescence-associated secretory phenotype induces cellular plasticity and tissue regeneration. Genes Dev 2017;31.

Robinson NA, LaCelle PT, Eckert RL. Involucrin is a covalently crosslinked constituent of highly purified epidermal corneocytes: evidence for a common pattern of involucrin crosslinking in vivo and in vitro. J Invest Dermatol 1996;107:101−7.

Röck K, Tigges J, Sass S, Schütze A, Florea AM, Fender AC, et al. miR-23a−3p causes cellular senescence by targeting hyaluronan synthase 2: possible implication for skin aging. J Invest Dermatol 2015;135:369−77.

Schosserer M, Grillari J, Breitenbach M. The dual role of cellular senescence in developing tumors and their response to cancer therapy. Front Oncol 2017;7:278.

Setzer SV, Calkins CC, Garner J, Summers S, Green KJ, Kowalczyk AP. Comparative analysis of armadillo family proteins in the regulation of A431 epithelial cell junction assembly, adhesion and migration. J Invest Dermatol 2004;123:426−33.

Sonkoly E, Wei T, Pavez Loriè EP, Suzuki H, Kato M, Törmä H, et al. Protein kinase C-dependent upregulation of miR-203 induces the differentiation of human keratinocytes. J Invest Dermatol 2010;130:124−34.

Szabowski A, Maas-Szabowski N, Andrecht S, Kolbus A, Schorpp-Kistner M, Fusenig NE, et al. C-Jun and JunB antagonistically control cytokine-regulated mesenchymal-epidermal interaction in skin. Cell 2000;103:745−55.

Takasugi M, Okada R, Takahashi A, Virya Chen D, Watanabe S, Hara E. Small extracellular vesicles secreted from senescent cells promote cancer cell proliferation through EphA2. Nat Commun 2017;8:15729.

Terlecki-Zaniewicz L, Lämmermann I, Latreille J, Bobbili MR, Pils V, Schosserer M, et al. Small extracellular vesicles and their miRNA cargo are anti-apoptotic members of the senescence-associated secretory phenotype. Albany NY: Aging; 2018.

Tokuyasu KT. A technique for ultracryotomy of cell suspensions and tissues. J Cell Biol 1973;57:551−65.

Urbanelli L, Buratta S, Sagini K, Tancini B, Emiliani C. Extracellular vesicles as new players in cellular senescence. Int J Mol Sci 2016;17.

Velarde MC, Demaria M. Targeting senescent cells: possible implications for delaying skin aging: A mini-review. Gerontology 2016;62:513−8.

Waaijer MEC, Gunn DA, Adams PD, Pawlikowski JS, Griffiths CEM, van Heemst D, et al. P16INK4a positive cells in human skin are indicative of

local elastic fiber morphology, facial wrinkling, and perceived age. J Gerontol A. Biol Sci Med Sci 2016;71:1022−8.

Wäster P, Eriksson I, Vainikka L, Rosdahl I, Öllinger K. Extracellular vesicles are transferred from melanocytes to keratinocytes after UVA irradiation. Sci Rep 2016;6:27890.

Watt FM, Green H. Involucrin synthesis is correlated with cell size in human epidermal cultures. J Cell Biol 1981;90:738−42.

Weilner S, Schraml E, Wieser M, Messner P, Schneider K, Wassermann K, et al. Secreted microvesicular miR-31 inhibits osteogenic differentiation of mesenchymal stem cells. Aging Cell 2016;15:744−54.

Yan C, Grimm WA, Garner WL, Qin L, Travis T, Tan N, et al. Epithelial to mesenchymal transition in human skin wound healing is induced by tumor necrosis factor-alpha through bone morphogenic protein-2. Am J Pathol 2010;176:2247−58.

Yosef R, Pilpel N, Tokarsky-Amiel R, Biran A, Ovadya Y, Cohen S, et al. Directed elimination of senescent cells by inhibition of BCL-W and BCL-XL. Nat Commun 2016;7:11190.

Zhou L, Wang H, Jing J, Yu L, Wu X, Lu Z. Regulation of hair follicle development by exosomes derived from dermal papilla cells. Biochem Biophys Res Commun 2018;500:325−32.

SUPPLEMENTARY MATERIALS AND METHODS

Full thickness human skin equivalents

A total of 2.5×10^5 human dermal fibroblasts were seeded in a collagen gel consisting of eight parts collagen G (Biochrom, Berlin, Germany), one part $10 \times$ HBSS (Thermo Fisher Scientific, Waltham, MA), and one part fetal calf serum (Sigma-Aldrich, St. Louis, MO) to form the dermis of human skin equivalents. The gel was equilibrated overnight with KGM-2 supplemented with KGM-2 Bullet Kit (Lonza, Basel, Switzerland) followed by a keratinocyte overlay of 1.5×10^6 cells on day 2. On day 3 they were lifted to the air-liquid interface to start differentiation using differentiation media (KGM, Lonza) supplemented with 1.15mM $CaCl_2$ (Sigma-Aldrich), 50 µg/ml L-ascorbic acid (Sigma-Aldrich), 0.1% BSA (Sigma-Aldrich), 10 µg/ml transferrin (Sigma-Aldrich), and the KGM BulletKit (Lonza) except bovine pituitary extract. The media was refreshed every other day throughout the whole differentiation process. On day 10, dermis (fibroblasts) and epidermis (keratinocytes) were harvested for RNA extraction.

Senescence-associated ß-Gal staining

Senescent fibroblasts and corresponding subconfluent non-stressed fibroblast at the middle of their replicative lifespan were stained according to the standard protocol described. Quantification was performed in a blinded and randomized fashion. Senescence-associated ß-Gal positive and negative cells from 15 images per well were counted.

miRNA transfection

Keratinocytes in passage 3/PD4.5 were reverse transfected with pre-miR-23a-3p (AM17100; Ambion, Foster City, CA) and scrambled control pre-miR-Ctrl#2 (AM 17111; Thermo Scientific) using siPORT NeoFX transfection agent (AM4511; Thermo Scientific). Per six well 2×10^4 to 3×10^4 cells/cm^2 (donor dependent) were transfected using 5 µl lipids and 30 nM final concentration of respective pre-miRNAs. Twenty-four hours post transfection, cells received a media change.

Similarly, fibroblasts in PD < 25 were transfected with *C. elegans*—specific cel-miR-39 and scrambled control pre-miR-Ctrl#2 (AM 17111; Thermo Scientific) using siPORT NeoFX transfection agent (AM4511; Thermo Scientific). Twenty-four hours post transfection, either fetal calf serum depleted media was added or the cells were harvested for embedding into skin equivalents.

RNA Isolation

Cells and small extracellular vesicles. Cells and small extracellular vesicles fractions from conditioned media were lysed in TRI Reagent (Sigma) and RNA was isolated according to the manufacturer's protocol. RNA concentration and quality was controlled using Nanodrop spectrometer (ND-1000). To monitor isolation efficiency of small extracellular vesicles-RNA, spike-ins (203203, UniSp2, UniSp4, UniSp5; Exiqon, Vedbaek, Denmark) were added before RNA isolation and RNA was extracted using the miRNeasy Mini kit (217004; Qiagen, Hilden, Germany) according to the manufacturer's instructions.

From dermis and epidermis of human skin equivalents.. Dermal and epidermal layers of human skin equivalents were separated and resuspended in 500 µL TRIzol reagent. Samples were homogenized for 30 seconds using pellet pestles (Z359947; Sigma) on ice, followed by sonication for 30 cycles (30 seconds sonication and 30 seconds hold). Subsequent RNA isolation was performed according to the standard protocol used for routine RNA isolation.

cDNA synthesis

For miRNA quantification. Equal volumes of vesicular-RNA and 10 ng of total RNA were used for cDNA synthesis using Universal cDNA Synthesis Kit II (Exiqon). UniSp6 control was included in small extracellular vesicle samples (Exiqon) to control for enzyme activity. cDNA was synthesized at 42 °C for 60 minutes, followed by 5 minutes at 95 °C.

For mRNA quantification. cDNA was synthesized from 500 ng of total RNA with the High-Capacity cDNA Reverse Transcription Kit including RNAse inhibitor (Applied Biosystems, Foster City, CA) for 10 minutes at 25 °C, 120 minutes at 37 °C, 5 minutes at 85 °C.

Quantitative reverse transcriptase in real time (QPCR)

miRNA QPCR analyses were performed using ExiLENT SYBR Green master mix and LNA-enhanced miRNA primer (Exiqon). QPCR for mRNA was performed with 5x HOT FIREPol EvaGreen QPCR Mix Plus with ROX (Medibena, Austria). All experiments were performed on a Rotor-GeneQcycler.

Intracellular miRNA expression was quantified using the ddCt method using U6 as a housekeeper.

Because of the absence of a robust vesicular housekeeping miRNA, we decided to use standardized secretion times and equal working volumes for all subsequent steps and normalized raw Ct values to total viable cell number of each sample. For better visualization, Ct values were further transformed to arbitrary units by assuming a Ct value of 40 to be 10 arbitrary units. Arbitrary units are presented as absolute values.

QPCR for mRNA expression levels was performed with 5x HOT FIREPol EvaGreen QPCR Mix Plus with ROX (Medibena) using a Rotor-GeneQcycler. Copy number was determined according to standard curves in duplicates. Samples were pipetted in quadruplicates and normalized to respective housekeeper genes to calculate fold changes. As reference genes we selected glyceraldehyde-3-phosphate dehydrogenase (GAPDH) for fibroblasts and B2M for keratinocytes. All negative controls tested were below detection limit of QPCR (>40).

Primers used for QPCR are the following: B2M sense: GAGATGTCTCGCTCCGTGG, B2M as: TACATGTCTC GATCCCACTTAAC; GAPDH sense: CGACCACTTTGT CAAGCTCA, GAPDH as: TGTGAGGAGGGGAGATTCAG; E-cadherin sense: CCCACCACGTACAAGGGTC, E-cadherin as: CTGGGGTATTGGGGGCATC; Plakophilin4/p0071 sense: AGGCTTGGAGCAGAATCACC, Plakophilin4/p0071 as: CCCTCACTTTCATGGAGAGATGT; VIM sense: GGAGTC CACTGAGTACCGGA, VIM as: GCTTCAACGGCAAAGTTCTC.

Protein quantification, western blot, and antibodies

Crude skin section extracts or extracellular vesicles enriched from skin sections by tangential flow filtration with a 300 kDa cut-off or size exclusion chromatography, as well as tangential flow filtration flow through, were directly combined with 4 × SDS loading dye (240 mM Tris/HCl, pH 6.8, 8% SDS, 40% glycerol, 0.05% bromophenolblue, 5% ß-Mercaptoethanol) after Pierce BCA Protein Assay Kit (23227; Thermo Scientific) or nanoparticle tracking analysis, heated to 95 °C for 10 minutes and subsequently sonicated. Cell pellets of human dermal fibroblasts were lysed in 1 × TNE buffer (2 × TNE: 100 mM Tris/HCl, pH 8.0, 300 mM NaCl, 1 mM EDTA, 2% Triton X-100) or RIPA buffer (150 mM NaCl, 1% NP-40 substitute, 0.5% deoxycholic acid, 0.1% SDS, 20% SDS, 50 mM Tris, pH 8.0) and protein concentration was quantified using the Pierce BCA Protein Assay Kit (23227; Thermo Scientific) according to manufacturer's recommendations. For SDS-PAGE and subsequent western blotting, samples were resuspended in SDS loading dye, heated to 95 °C, and sonicated. Samples were separated either on a NuPAGE 4−12% Bis/Tris polyacrylamide gel (10472322; Invitrogen/Thermo Scientific) or on a 15% Mini-PROTEAN TBE Gel (4565054; Biorad, Hercules, CA) at 200 V and proteins were transferred to a PVDF membrane (170−4156; Biorad) in a Biorad SemiDry Blotting System at 1.3A, 25 V for 7 minutes. After blocking with either 3% milk or 2.5% BSA in 1 × PBS with 0.1% Tween-20 (P2287; Sigma-Aldrich GmbH) for 1 hour, membranes were incubated with primary antibodies in blocking buffer (see below). Proteins were detected using secondary antibodies for IRDye 800CW donkey anti-rabbit IgG, 0.5 mg (926-32213; LI-COR Biosciences, Lincoln, NE), and IRDye 680RD donkey anti-mouse IgG, 0.5 mg (926-68072; LI-COR Biosciences), with a 1:10000 dilution using the Odysee (LI-COR Biosciences) infrared image system. In 2.5% BSA: TSG101 1:2000 (ab125011; Abcam), syntenin 1:1000 (TA504796; Origene, Rockville, MD), calnexin 1:1000 (ab22595; Abcam). In 3% milk: GAPDH 1:1000 (sc-25778; Santa Cruz, Dallas, TX) and involucrin 1:1000 (MA5-11803; Thermo Fisher).

Nanoparticle tracking analysis

The Zetaview system (Particle Metrix, Meerbusch, Germany) was used for determination of size and concentration of extracellular vesicles. The system was calibrated using 110 nm polystyrene standard beads (Particle Metrix, Meerbusch, Germany). Camera sensitivity was adjusted to fit the highest and lowest concentrated sample and all samples were measured with the same dilution and settings. Settings were the following: Gain 904, 98; Offset 0; 30 frames per seconds. Measurements were taken at 11 different camera positions and analysis was performed with software version 8.04.02.SP1. In case of pooled and concentrated size exclusion chromatography fractions from dISF samples, we used the Nanosight NS300 (Malvern Panalytical, Malvern, United Kingdom) under the following conditions: Temperature, 25 °C; Syringe Pump Speed/Arbitrary units, 50; Camera type, sCMOS; Laser Type, Blue488; number of videos, as stated in figure legend; video duration, 60 seconds; samples were minimally diluted.
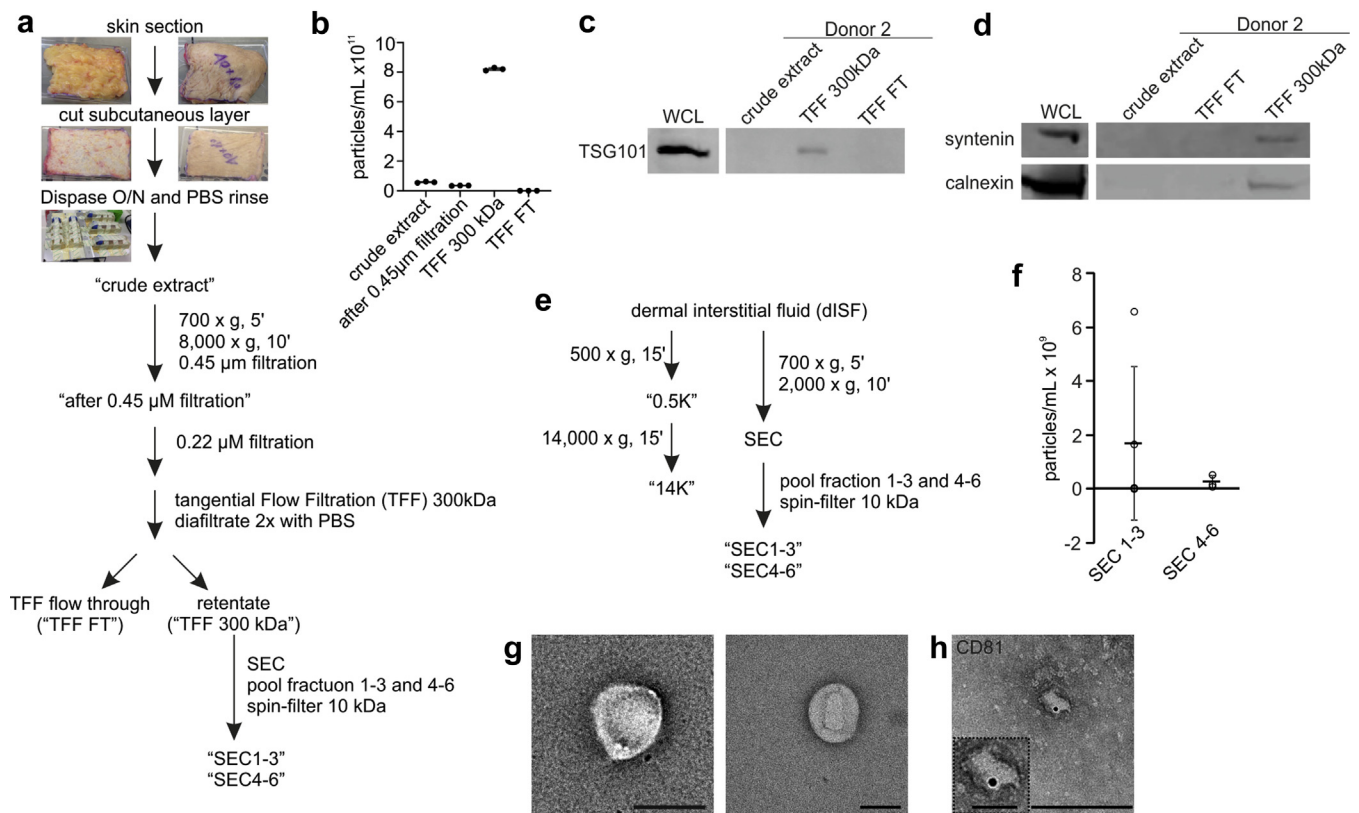
Supplementary Figure S1. Extracellular vesicles are present in the human skin. (**a**) Scheme of sEV purification from skin sections. Subcutaneous fat layer was removed. Skin sections were cut into small pieces, digested with dispase overnight (O/N), and rinsed with PBS. Solvents were collected making up the crude extract. After differential centrifugation, the crude extract was filtered through various pore sizes (0.45 μm and 0.22 μm) and subjected to tangential flow filtration with a cut-off of 300 kDa. The retentate was further purified using SEC. Fractions 1−3 and 4−6 were pooled and concentrated with 10 kDa spin-filters. (**b**) Particles in crude extract from skin sections are enriched by subsequent 0.45 μm filtration and TFF (300 kDa) as determined by NTA. Each sample was measured in technical triplicates. (**c**) Western blot analysis of crude extract and enriched sEVs by TFF (TFF 300 kDa) from human skin sections for EV-specific protein TSG101. Whole cell lysate from human dermal fibroblasts was used as a positive control, TFF flow through as a negative control. (**d**) Western blot analysis of crude extract and enriched sEVs by TFF (TFF 300 kDa) from human skin sections for EV-specific protein syntenin and non-EV marker calnexin. Whole cell lysate from human dermal fibroblasts was used as a positive control, TFF flow through as a negative control. (**e**) Scheme of EV purification from dISF. Samples were either subjected to two centrifugation steps at 0.5K and 14K*g* and supernatants analyzed or EVs were purified by SEC after two short centrifugation steps. SEC fractions 1 to 3 and 4 to 6 were pooled and concentrated by 10 kDa spin-filters. (**f**) EVs isolated from dISF by differential centrifugation and subsequent SEC were analyzed by NTA, revealing a very low particle count (concentration warning in all videos). SEC fractions 1−3 and 4−6 were pooled and concentrated using 10 kDa spin-filters. SEC 1−3 was measured in five videos and SEC 4−6 in three videos. (**g**) TEM images of EVs purified from dISF samples by differential centrifugation and subsequent SEC. Images show EVs in pooled SEC fractions 1−3, which were concentrated by 10 kDa spin-filters. Scale bar = 100 nm. (**h**) TEM images of EVs purified from dISF samples by differential centrifugation and subsequent SEC. Images show EVs positive for EV marker CD81 by immunogold labeling in pooled SEC fractions 1−3, which were concentrated by 10 kDa spin-filters. Scale bar = 200 nm and 50 nm (region of interest). dISF, dermal interstitial fluid; EV, extracellular vesicle; NTA, nanoparticle tracking analysis; PBS, phosphate buffered saline; SEC, size exclusion chromatography; sEV, small extracellular vesicle; TEM, transmission electron microscopy; TFF, tangential flow filtration.

Figure S2. Characterization of stress-induced premature senescence. (**a**) Representative western blot shows expression of the cell cycle inhibitor p21 in non-treated Q and SIPS cells. p21 levels were normalized to GAPDH as a housekeeper. (**b**) Representative morphology of Q and SIPS cells after 2 weeks recovery post last stress treatment. Scale bar = 200 µm. (**c**) Significant increase of SA-ß-Galactosidase (SA-ß-Gal) in SIPS cells after 4, 11, and 18 days post last stress treatment compared with young (PD10) proliferating cells. A total of 15 pictures were taken randomly at a magnification of ×10 and counting was performed in blinded fashion. Percentages of SA-ß-Gal positive cells from all images were calculated. Averages from one donor in triplicates are shown ± SEM from raw values. $*P < 0.05$, $**P < 0.01$; tested against young PD10. Statistical analysis was performed using one-way ANOVA following Tukey's multiple comparison test. (**d**) Representative image of SA-ß-Galactosidase staining of proliferating (young PD10) and senescent (SIPS) fibroblasts 4 days post last stress treatment. Scale bar = 200 µm. ANOVA, analysis of variance; GAPDH, glyceraldehyde-3-phosphate dehydrogenase; Q, quiescent; SA, senescence-associated; SEM, standard error of the mean; SIPS, stress-induced premature senescent.

a

Q sEV   SIPS sEV

b

c

d

miR-Ctrl   miR-23a-3p
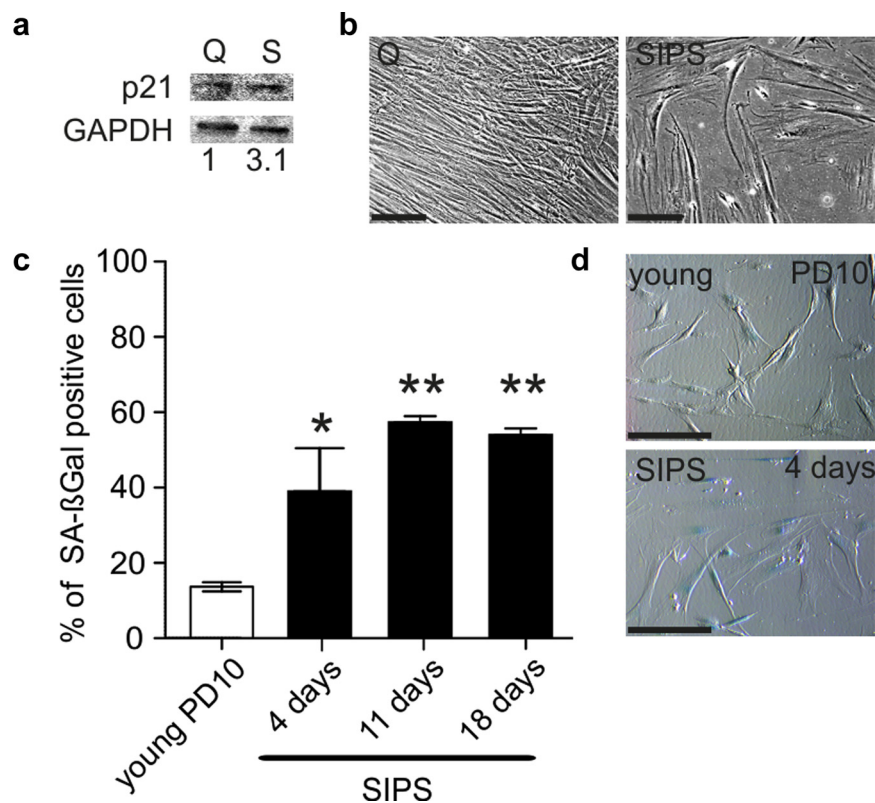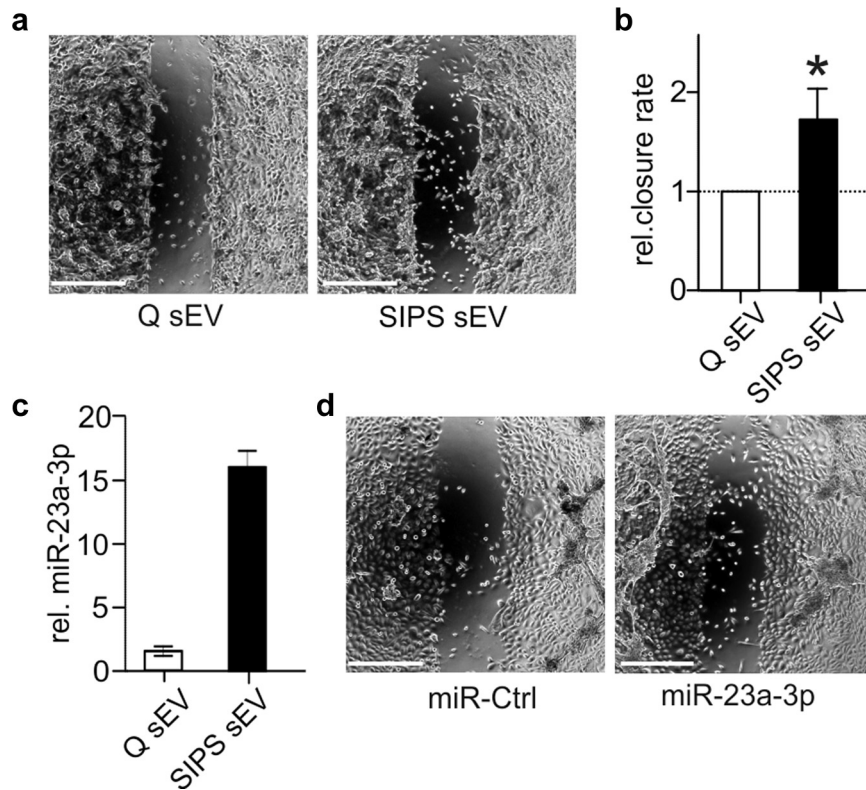
Supplementary Figure S3. sEVs from senescent HDFs and miR-23a-3p overexpression enhance wound/gap closure of keratinocytes. (**a**) Representative images of culture inserts show keratinocytes growing into the gap of the cell monolayer after exposure to senescent or quiescent control derived sEVs. Scale bar = 400 μm. (**b**) Relative closure rate determined in scratch assays of keratinocytes exposed to SIPS or Q derived sEVs. Closure rate was calculated using first and last timepoint and was normalized to Q control. Bar chart shows mean ± SEM values from six independent experiments, with sEVs from three different fibroblast donors and three different donors of recipient keratinocytes. *$P < 0.05$; Wilcoxon signed rank test. (**c**) miR-23a-3p levels in sEVs of senescent and quiescent fibroblasts after 3 weeks post stress treatment. Raw Ct values of miR-23a-3p were normalized to the number of cells used for sEV purification, and arbitrary units were calculated from Ct values by assuming a Ct value of 40 to be 10 AU. Data of three biological replicates ± SEM are presented. (**d**) Representative images of 2D culture dishes show keratinocytes transfected with miR-23a-3p or respective miR-Ctrl growing into the gap. Scale bar = 400 μm. AU, arbitrary units; HDF, human dermal fibroblast; Q, quiescent; SEM, standard error of the mean; sEV, small extracellular vesicle; SIPS, stress-induced premature senescent.